CFD-DEM SIMULATION OF A BUBBLING FLUIDIZED BED

Lucilla Coelho de Almeida, lucillalmeida@gmail.com[1,2]
João Américo Aguirre Oliveira Junior, aguirre@esss.com.br[2]
Jian Su, sujian@nuclear.ufrj.br[1]

[1]Nuclear Engineering Program, COPPE, Universidade do Federal do Rio de Janeiro, 21941-972, Rio de Janeiro - RJ - Brasil
[2]Engineering Simulation and Scientific Software, ESSS, Av. Presidente Vargas, 3131, 20210-031, Rio de Janeiro - RJ - Brasil

Abstract: *Several conceptual designs of the fluidized-bed nuclear reactor have been proposed due to advantages over conventional nuclear reactors, amongst which the enhanced heat transfer and mixing, reduced risk of hot-spot, higher burn-up of the fuel and increased safety. Accurate modeling of the particles and the coolant behavior is required to reliably evaluate the thermo-hydraulic efficiency and margin of safety of these reactors. The two-way coupling between solid and fluid can account for high-fidelity solid-solid interaction and reasonable accuracy in fluid calculation and fluid-solid interaction. In this work, particles are modeled as a discrete phase following the DEM approach, while the fluid is treated as a continuous phase, described by the volume averaged Navier-Stokes equations. The numerical approach was applied to the simulation of a bubbling fluidized bed and the pressure drop results were compared to experimental data, showing good agreement. The evaluation of the bed dynamics showed that the model was able to reproduce the expected behavior of a bubbling fluidized bed formed by Geldart D particles and confirmed the particle temperature uniformity within the bed.*
Keywords: *CFD-DEM, Fluidized bed, Nuclear reactor*

1. INTRODUCTION

Fluidized beds are widely used in many plant operations in chemical, energy production, oil and gas, mineral and agricultural industries, mainly due to good mixing characteristics and high contact surface area between gas and solid phases. Various conceptual designs of the fluidized-bed nuclear reactor have been proposed and their feasibility demonstrated (Sefidvash, 1985; Sefidvash, 1980; Agung, 2007), due to advantages over conventional nuclear reactors, amongst which the enhanced heat transfer and mixing, reduced risk of hot-spot, higher burn-up of the fuel and increased safety. In general, a fluidized bed nuclear reactor consists of a graphite-walled tube partially filled with coated fuel particles, arranged in the bottom part of the cavity, forming a packed bed. The coolant flows from bottom to top through the tube, thereby fluidizing the particle bed.

In order to improve the design and scale-up of fluidized beds reactors it is critical that the hydrodynamics and transport phenomena that occur in these systems are known. Despite their widespread application in both chemical and nuclear industries, much of the development and design of fluidized bed reactors has been empirical as the complex flow behavior of gas–solid flow in these systems makes flow modeling a challenging task (Taghipour *et al.*, 2005). With the increase in computational power, computational modeling of fluidized beds have been increasingly held as suitable to provide complete information of granular flows (Chiesa *et al.*, 2005; Deen *et al.*, 2007; der Hoef *et al.*, 2006), making it possible to observe these systems with a wealth of details infeasible to be obtained experimentally, without the use of invasive techniques and enabling the measuring of fluid and particles properties simultaneously. Moreover, the use of computational tools allows evaluation of different operating conditions and geometrical configurations without the need to build experimental prototypes (or at least reducing their number), substantially reducing the cost and design time.

The major difficulty in the modeling of fluidized beds is the large-scale of lengths existing in the system, since the major structures are order of magnitude of the device, ie meters, while the momentum, heat and mass transfer occur in the micrometric scale of the interactions between particles and particle-gas. Existing approaches for describing hydrodynamics of the gas and particulate phases can be classified into two categories in view of the particulate phase: continuous approach, at the macroscopic level and the discrete approach, at the particles level. At the macroscopic level, the fluid and solid phases are treated as continuous and interpenetrating in a computational cell that is much larger than the individual particles, but still small compared to the size of process scale. Adopting location-based averaging techniques, local media variables are used in the conservation equations, which are in turn resolved through computational fluid dynamics (CFD). The advantage of this approach is its reasonable computational cost for practical application problems, making the most currently used for modeling processes fluidization (Gidaspow, 1994). However, besides being unable to provide individual particles flow information, the capacity of continuous approach to produce good results is directly dependent on the constitutive relations adopted for modeling interactions between the phases and the rheology of the particulate material.

The Distinct Element Method (DEM), initially proposed by Cundall and Strack (1979) refers to the application of the discrete particles method (DPM) in granular systems (Xu and Yu, 1997). In the discrete approach, the movement of the particles is directly obtained by numerical integration of the equations that govern the translation and rotation of each of the particles in the system. By taking into account the interactions that occur in the system (fluid-particle, particle-particle and particle-wall), the discrete approach can be used to represent the interactions of the particulate phase at larger scales

(der Hoef *et al.*, 2006) and produce close relations to the macroscopic approach.

The spatial scales for solving the fluid flow may also vary from smaller than the particle, which can be discrete (as in the case of coupling Lattice-Boltzmann method with DEM) or continuous (such as coupling Direct Numerical Simulation (DNS) with DEM) to the magnitude of the computational cell. The sub-particles models, despite being very expensive computationally and thus unfeasible for practical applications in engineering, are of great value due to its ability to determine the interaction forces between the fluid and particles.

The coupled CFD-DEM approach is a promising alternative for modeling granular-fluid systems, introduced by early developers (Tsuji *et al.*, 1993; Hoomans *et al.*, 1996; Xu and Yu, 1997) and lies in an intermediate level between adopting the sub-particle resolution to the fluid and particle phase (like DNS-DEM coupling) and using the cell resolution for both particle and fluid phases (as in the case the continuous models based on granular kinetic theory). In the CFD-DEM model, the particles are modeled as a discrete phase, following the DEM approach, whereas the fluid flow is treated as a continuous phase, described by the averaged Navier-Stokes equations on a computational cell scale (Drew, 1993).

This approach has been recognized as an effective method to study particle–fluid flows (Zhu *et al.*, 2008) and its applicability for modeling fluidized beds has been verified through comparison with experimental results, which have shown promising results. A fairly complete review of the modeling of fluidized beds using DPM can be found in the work of Deen *et al.* (2007).

The DEM-CFD coupling has been used to study the bubbles dynamics in fluidized beds, including their formation, coalescence and breakage (Yuu *et al.*, 2000; Ouyang and Li, 2001; Xu and Yu, 1997; Xu *et al.*, 2000). Goldschmidt *et al.*, 2002, Goldschmidt *et al.*, 2004 and Chiesa *et al.*, 2005 compared the results obtained using the coupling between DPM with CFD and using the two-fluids model with experimental results of fluidized beds and reported better agreement using the Lagrangian approach, despite the greater computational cost.

A series of studies analyzing the effect of the particles' and gas' properties in the fluidization was published by Ye *et al.*, 2004, Ye *et al.*, 2005b and Ye *et al.*, 2005a. Hoomans *et al.* (2001) used the DEM-CFD coupling to study a fluidized bed and emphasized the importance of the collision parameters for the accurate reproduction of experimental data.

Hoomans *et al.* (2000) used the Euler-Lagrange approach to evaluate particles segregation as function of their sizes and densities in a fluidized bed. Bokkers *et al.* (2004) subsequently applied this model to evaluate the separation of binary mixtures of particles, obtaining good agreement with experimental results. Recently, Luo *et al.* (2015) published a study using CFD-DEM coupling to study the mixing and dispersion of particles in a fluidized bed under different fluid flow rates.

The heat transfer during fluidization is of great industrial importance and CFD-DEM coupling together with appropriate model for heat transfer has been recently used to study the heat transfer mechanisms in fixed or fluidized beds, such as Zhou *et al.*, 2006, Zhou *et al.*, 2007 and Zhou *et al.*, 2010. Patil *et al.* (2014) adopted DEM to study the non-isothermal effects on the formation and rise of bubbles in fluidized beds, obtaining good results for small particles when compared to experimental results.

In this work, coupling between DEM package Rocky® and CFD package Fluent® will be demonstrated. The proposed approach was applied to the simulation of a bubbling fluidized bed including heat transfer between particles and particles and fluid. The numerical results were compared to experimental data and showed good agreement.

2. MODEL DESCRIPTION

In this section, governing equations for the fluid and solid phases are provided and the coupling methodology is described in details. The fluid flow is obtained by the conventional continuum approach using ANSYS Fluent®, in which the conservation equations for mass, momentum and energy are solved by the finite volume method. The solid phase flow is modeled using the discrete approach within Rocky. The coupling between solid and fluid is accomplished by interphase momentum and heat transfer terms due to the interaction between phases.

2.1 Particle phase modeling

All particles within the computational domain are tracked in a Lagrangian way, by solving the equations that governs translational (Eq. (1)) and rotational particle motion (Eq. (2)).

$$m_p \frac{d\mathbf{v}_p}{dt} = \mathbf{F}_c + \mathbf{F}_{f\to p} + m_p \mathbf{g} \tag{1}$$

$$\mathbf{J}_p \frac{d\omega_p}{dt} = \mathbf{M} \tag{2}$$

where m_p is the particle mass, $\mathbf{g}$ is the gravitational acceleration vector, $\mathbf{F}_c$ is the contact force that accounts for particle-particle and particle-wall interactions, ω_p is the angular velocity vector, $\mathbf{J}_p$ is its moment of inertia, $\mathbf{M}$ is the net torque generated by tangential forces that causes the rotation of the particle and $\mathbf{F}_{f\to p}$, is the additional force accounting for the interaction with the fluid phase, which calculation is further described in section 2.3

Following the soft sphere approach, in which the particles can overlap slightly during the contact and the contact force is calculated based on this overlap, the contact force, $\mathbf{F}_c$, is decomposed into two orthogonal components, consisting of

the normal force, $\mathbf{F}_N$, and the tangential force, $\mathbf{F}_T$. The normal contact force, $\mathbf{F}_N$, is calculated according to the Equation 3, using a hysteretic linear spring model (Walton (1993)).

$$\mathbf{F}_N = \begin{cases} \min\left(\mathbf{F}_N^0 + K_U\Delta\delta, K_L\delta\right) & \text{for } \Delta\delta \geq 0 \\ \max\left(\mathbf{F}_N^0 + K_U\Delta\delta, 0.001K_L\delta\right) & \text{for } \Delta\delta < 0 \end{cases} \tag{3}$$

where $\mathbf{F}_N^0$ is the normal contact force of the previous time step and K_L e K_U are the loading and unloading stiffness. $\Delta\delta$ is the difference between the current normal overlap on collision, δ, and the overlap of the previous time step. The particle stiffness is calculated accroding to Eq. 4 .

$$K_i = E_i d_i \tag{4}$$

The loading stiffness, K_L, and unloading stiffness, K_U, are calculated as functions of the stiffness of the particles (K_i, K_j) and the restitution coefficient of the contacting pair, ε, as shown in Equation 5 and Equation 6.

$$K_L = \frac{K_i K_j}{K_i + K_j} \tag{5}$$

$$K_U = \frac{K_i K_j}{(K_i + K_j)\,\varepsilon^2} \tag{6}$$

For the tangential force calculation, $\mathbf{F}_T$, a elastic-frictional model is adopted, as shown in Equation 7:

$$\mathbf{F}_T = \begin{cases} \min\left(\mathbf{F}_T^0 + K_L ds_T, \eta_{st}\mathbf{F}_N\right) & \text{if slipping} \\ \max\left(\mathbf{F}_T^0 + K_L ds_T, \eta_d\mathbf{F}_N\right) & \text{otherwise} \end{cases} \tag{7}$$

where $\mathbf{F}_T^0$ is the tangential contact force of the previous time step, ds_T tangential displacement during contact, η_{st} is the static friction coefficient and η_d is the dynamic friction coefficient.

An additional equation for the energy balance is solved along with the equations governing the motion of the particle. In the current implementation, the particle temperature is assumed uniform, i.e., no radial or circumferential temperature variation is admitted. This approximation is reasonable for small or highly conductive particles. The temperature variation of a particle can be obtained over time according to the Eq. 8:

$$m_p c_p \frac{dT_p}{dt} = q_c + q_{f\to p} \tag{8}$$

where c_p is the specific heat of the particle material. This heat transfer rate accounts for the heat transfer that occurs during the contact with other particles or walls, q_c, and the heat transfer between particle and fluid phase, $q_{f\to p}$, whose calculations are shown in Section 2.4

2.2 Fluid phase modeling

The fluid phases are described by the classical Navier-Stokes equations averaged in volume Drew (1993). The averaged mass conservation equation is given by Eq. (9) whereas the momentum conservation equation is written as Eq. (10), where α_f stands for the fluid volume fraction, p is the shared pressure, ρ_f is the fluid density, $\mathbf{u}_f$ is the fluid phase velocity vector and $\mathbf{T}_f$ is the stress tensor of fluid phase.

$$\frac{\partial}{\partial t}\left(\alpha_f\rho_f\right) + \nabla\cdot\left(\alpha_f\rho_f\mathbf{u}_f\right) = 0 \tag{9}$$

$$\frac{\partial}{\partial t}\left(\alpha_f\rho_f\mathbf{u}_f\right) + \nabla\cdot\left(\alpha_f\rho_f\mathbf{u}_f\mathbf{u}_f\right) = -\alpha_f\nabla p + \nabla\cdot\left(\alpha_f\mathbf{T}_f\right) + \alpha_f\rho_f\mathbf{g} + \mathbf{F}_{p\to f} \tag{10}$$

In order to describe energy conservation, a separate enthalpy equation is written for each fluid phase, according to Eq. (11), where h_f is the specific enthalpy of the fluid phase, $\mathbf{q}_f$ is the heat flux and $Q_{p\to f}$ is the heat exchange between fluid and particulate phases.

$$\frac{\partial}{\partial t}\left(\alpha_f\rho_f h_f\right) + \nabla\cdot\left(\alpha_f\rho_f\mathbf{u}_f h_f\right) = \alpha_f\frac{\partial p_f}{\partial t} + \alpha_f\mathbf{T}_f : \nabla\mathbf{u}_f - \nabla\cdot\mathbf{q}_f + Q_{p\to f} \tag{11}$$

In Eq. (10), $\mathbf{F}_{p\to f}$ represents the source term of momentum from interaction with the particulate phase, calculated according to Eq. (12), where V_C is the computational cell volume and $\mathbf{F}_{f\to p}$ accounts for the forces generated by the fluid on the particles, calculated according to the section 2.3

$$\mathbf{F}_{p\to f} = -\frac{\sum_{p=1}^{N}\mathbf{F}_{f\to p}}{V_C} \tag{12}$$

The heat exchange with the particulate phase is analogously calculated according to Eq. 13, where $q_{f\to p}$ is the heat transfer rate between fluid and particle, which calculation is shown in section 2.4

$$Q_{p\to f} = -\frac{\sum_{p=1}^{N} q_{f\to p}}{V_C} \tag{13}$$

2.3 Particle-fluid interaction forces

The fluid interaction force, $\mathbf{F}_{f\to p}$, is in general splitted into the drag force, $\mathbf{F}_{\mathrm{D}}$, and a second term composed by the remaining (non-drag) forces, amongst which the most common are the pressure gradient force, the added (virtual) mass force and the lift force. Depending on the flow conditions, the majority of these forces can be neglected and only the drag and pressure gradient forces need to be considered. Therefore, in the current case, the fluid interaction force is calculated according to Eq. (14):

$$\mathbf{F}_{f\to p} = \mathbf{F}_{\mathrm{D}} + \mathbf{F}_{\nabla p} \tag{14}$$

The pressure gradient force, $\mathbf{F}_{\nabla p}$, is calculated according to the Eq. (15):

$$\mathbf{F}_{\nabla p} = -V_p \nabla p \tag{15}$$

where V_p is the volume of the particle and ∇p is the local pressure gradient.

The drag force, $\mathbf{F}_{\mathrm{D}}$, acting on the particles is calculated using the definition of the drag coefficient, C_D, (see Pritchard (2010)), according to Eq. (16), where $\mathbf{u}_f - \mathbf{v}_p$ is the relative velocity between particle and fluid and $A^{'}$ is the projected particle area in the flow direction.

$$C_D = \frac{\mathbf{F}_{\mathrm{D}}}{\frac{1}{2}\rho_f A^{'} \left|\mathbf{u}_f - \mathbf{v}_p\right| \left(\mathbf{u}_f - \mathbf{v}_p\right)} \tag{16}$$

The Huilin & Gidaspow correlation was adopted to calculate the the drag coefficient as given by Eq. (17). A blending function ψ, written in Eq. (18), is used to promote the connection based on the fluid volume fraction of the drag correlation developed by Wen & Yu (Gidaspow (2012)), given by Eq. (19), and the correlation developed by Ergun (Crowe *et al.* (2011)), given by Eq. (20).

$$C_{D_{\text{Huilin\&Gidaspow}}} = \psi C_{D_{\text{Ergun}}} + (1-\psi)\, C_{D_{\text{Wen\&Yu}}} \tag{17}$$

$$\psi = \frac{\arctan\left[150 \cdot 1.75\left(0.8 - \alpha_f\right)\right]}{\pi} + 0.5 \tag{18}$$

$$C_{D_{\text{Wen\&Yu}}} = \max\left\{\frac{24}{\alpha_f Re_p}\left[1 + 0.15\left(\alpha_f Re_p\right)^{0.687}\right]\alpha_f^{-1.65}, 0.44\alpha_f^{-1.65}\right\} \tag{19}$$

$$C_{D_{\text{Ergun}}} = 200\frac{\alpha_s}{\alpha_f \phi^2 Re} + \frac{7}{3\phi} \tag{20}$$

2.4 Heat transfer between particles and between particles and fuid

The heat exchanged during contact between particle i and a particle or wall j, $q_{c,ij}$, is calculated using a linear model as shown in Eq. (21), where $k_{c,ij}$ is the effective contact thermal conductivity.

$$q_{c,ij} = k_{c,ij} d_{c,ij}\left(T_j - T_i\right) \tag{21}$$

The contact diameter, $d_{c,ij}$, is considered much smaller than the geometric diameter of the contacting particles i and j, and is calculated according to (Chaudhuri *et al.*, 2006) using Eq. (22), where $\mathbf{F}_{N,ij}$ is the contact normal force between i and j and d_{ij} is the geometric mean of the colliding particles diameters. The contact equivalent Young's modulus, E_{ij}, is calculated according to Eq. (23), where σ is the Poisson ratio of the particle or wall.

$$d_{c,ij} = \left(\frac{4\mathbf{F}_{N,ij} d_{ij}}{E_{ij}}\right)^{\frac{1}{3}} \tag{22}$$

$$E_{ij} = \frac{4}{3}\frac{1}{\frac{1-\sigma_i^2}{E_i} + \frac{1-\sigma_j^2}{E_j}} \tag{23}$$

The heat transfer rate between a particle and fluid, $q_{f\to p}$, can be calculated using the Newton's law of cooling, given by Eq. (24), where T_p is the temperature of the particle's surface, T_f is the local fluid temperature and A_p is the particle surface area.

$$q_{f\to p} = hA_p\left(T_f - T_p\right) \tag{24}$$

The average convective heat transfer coefficient, h, is calculated based on the Nusselt number, *Nu*, by Eq. (25), where k_f is the fluid thermal conductivity.

$$h = \frac{Nu k_f}{d_p} \tag{25}$$

The empirical correlation of Gunn (1978), shown in Eq. (26), was used for calculating the Nusselt number, where *Pr* is the Prandtl number.

$$Nu = \left(7 - 10\alpha_f + 5\alpha_f^2\right)\left(1 + 0.7 Re_p^{0.2} Pr^{1/3}\right) + \left(1.33 - 2.4\alpha_f + 1.2\alpha_f^2\right) Re_p^{0.7} Pr^{1/3} \tag{26}$$

3. PROBLEM DESCRIPTION

3.1 Experimental facility

Experimental data of SSCP-I were obtained in a 7.62 cm x 22.86 cm x 121.92 cm bubbling fluidized bed with rectangular cross section, as illustrated in Fig. 1(a). The bed material for the experiment was Geldart group D particles of uniform size and high sphericity. A low frequency (1 Hz) transducer was used to measure the mean pressure drop across two heights, as can be seen in Fig. 1(b).

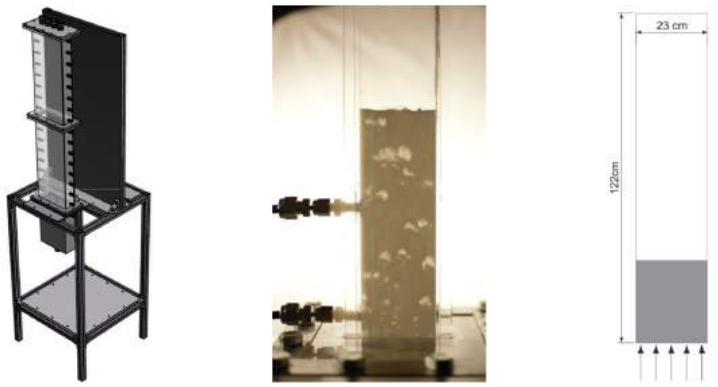

(a) (b) (c)

Figure 1: (a) SSCP-I test facility, (b) Experimental facility showing pressure intakes and (c) numerical domain.

3.2 Simulation set-up

The experimental system was modeled by a column with rectangular cross-section. The gas distributor was not included in the domain, so that the gas enters the domain through the bottom with uniform superficial velocity, as shown in Fig. 1(c) and $10°C$. The gas leaves the domain through the top, which is under atmospheric conditions. A uniform grid with an initial bed composed by 92949 spherical particles with diameter of 3.256 mm at $50°C$ and initial height of 16.4 cm was prescribed at the beginning of the simulation. The geometry and simulation set-up details are given in Tab. 1 .

In order to monitor the particles and pressure drop response to increasing gas flow rate, the superficial velocity of the gas was linearly increased from 0 to the target final velocity during 2 s and kept at this value after that. The time step of the DEM simulations for the linear hysteresis normal force model is defined by material stiffness, mass of particles and number of time step per loading cycle. The time step for the CFD simulations was recalculated as the closest value that is a multiple of the DEM time step, based on an initial time step.

Tabela 1: Domain, particle and gas properties.

	Property	**Value**	**Unit**
Domain	Domain size (W × D × H)	$23 \times 8 \times 123$	mm
	Grid cells	$24 \times 8 \times 124$	-
Particles	Equivalent diameter (d_p)	3.256	mm
	Density (ρ_p)	1131	kg/m^3
	Inventary mass	1.9	kg
	Particle-particle static and dynamic friction coefficients ($\eta_{st,p-p}$, $\eta_{d,p-p}$)	0.3	-
	Particle-walls static and dynamic friction coefficients ($\eta_{st,p-w}$, $\eta_{d,p-w}$)	0.35	-
	Particle-particle restitution coefficient (ε_{p-p})	0.92	-
	Particle-walls restitution coefficient (ε_{p-w})	0.92	-
	Particle Young's modulus (E_p)	10^7	N/m^2
	Initial temperature (T_p^0)	50.0	$°C$
Gas	Density (ρ_f)	1.20	kg/m^3
	Viscosity (μ_f)	$1.9E^{-05}$	$Pa.s$
	Inlet temperature (T_f^0)	10.0	$°C$
	Inlet superficial velocity (U_f)	$2.18E^{-05}$	m/s
	Time step (before correction)	$1E^{-03}$	s

4. Simulation results

4.1 Bed dynamics

In order to qualitatively assess the bed behavior before and after fluidization starts, particles were divided into seven different groups according to their initial positions, as can be seen in Fig. 2(a) and monitored over time. Figure 2(b) shows the moment in which fluidization is about to start, and as expected, virtually no activity is observed in the bed and particles remain about the same initial position and the bed height did not change.

Figure 2(c) shows the fluidization process with the gas superficial velocity gradually increase, while Fig. 2(d) shows the particles location at the moment in which final velocity is achieved. Bubbles formation can observed beyond minimum fluidization velocity, as shown in Fig. 2(e), confirming the expected bubbly regime characteristic for fluidized beds operation. Lastly, Fig. 2(f) displays the particles configuration after 5s of simulation, showing that particles are completely mixed, which confirms one of the main advantages of the used of the fluidized bed concept on nuclear reactors.

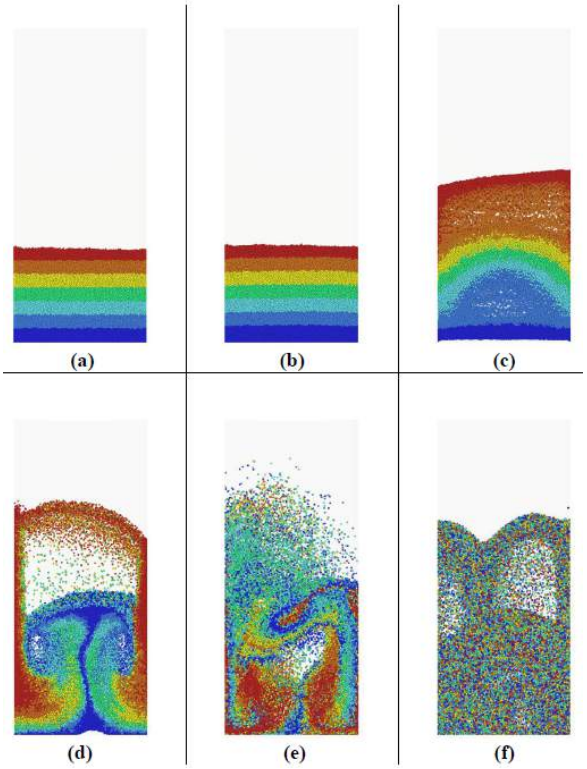

Figure 2: Evolution of particle behaviour with time.

4.2 Pressure drop analysis

The simulated pressure drop between the two pressure intake locations is shown in Fig.3 and compared to the averaged pressure drop value obtained experimentally (dashed lined). The fluctuating behavior of the pressure in a bubbling fluidized bed was captured by the simulation, which oscillates around a mean value which is close to the experimental average. Bokkers *et al.* (2004) reported that the use of a drag correlation combining the Ergun equation with the Wen and Yu overestimated the drag force and the bubble size, while the use of the Koch and Hill model (Koch and Hill (2001)) for calculating the drag coefficient produced results with a better agreement with the experiment.

At the same plot, the dotted line marks the moment at which the minimum fluidization velocity measured at experiments is achieved. It can be seen that it coincides well with the point at which the behavior of the pressure drop changes from linear to constant at simulation.

4.3 Particle velocity analysis

A dual recirculation pattern was observed when observing particles tracking along the simulation. The particles are carried in the front of the gas bubbles along the central area of the bed. Upon reaching the top, the particles move to the sides of the bed and then follow a downward path following the walls, returning to the central region, restarting the cycle. The same pattern was found in the work Luo *et al.* (2015).

In order to quantitatively compare with experimental results, in which the average velocity of the particles in five different regions of the bed (shown in Fig. 4(a)) was reported, the average velocity of the particles inside each one of these regions was obtained and then averaged between 2 and $10s$.

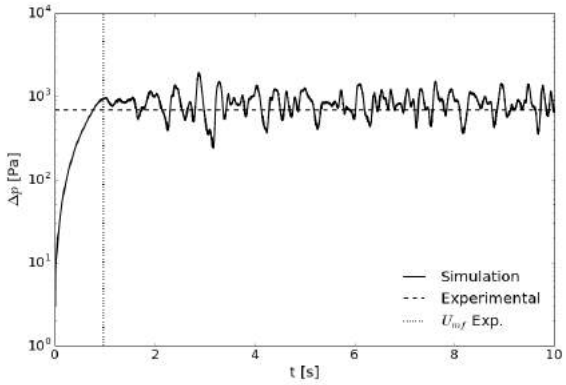

Figure 3: Comparison between simulation and experimental results of pressure drop between the two pressure intake locations.

Figure 4(b) shows that the vertical velocity profile obtained numerically has the same trend as the experimental one, with positive velocity in the central region where the bubbles carry particles upward and negative values in the regions near the walls, where the particles return to fill the empty region. The magnitude of the velocity is overestimated in the simulation. It is expected that the use of Koch and Hill drag law produces lower velocity values in such regions, since the drag force must be smaller.

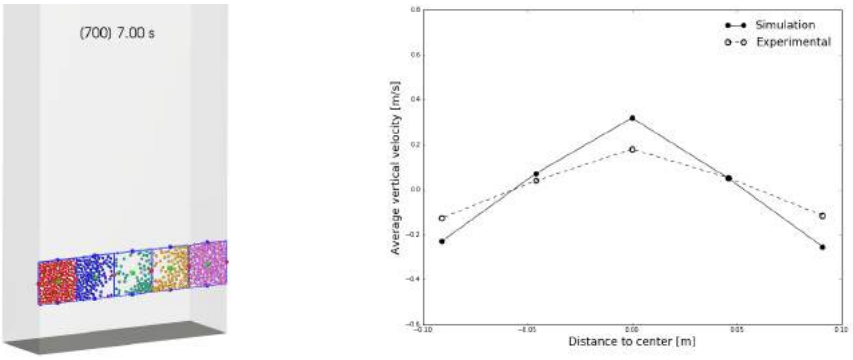

(a) (b)

Figure 4: (a) averaging bins and (b) vertical velocity profile.

4.4 Particle temperature analysis

Figure 5 shows particles colored by temperature at five different instants. At the first second of simulation, shown in Fig. 5(a), fluidization is about to start and particles are at the same position they were when the gas started to flow through the bed. It can be seen that the first layers of particles have lower temperature then the remaining bed, due to heat transfer with the flowing gas that enters the bed at $10°C$. This gas is heated and is not able to transfer heat with particles positioned higher in the bed.

After fluidization process has started, those particles that are in the bottom and have lower temperatures go to upper positions of the bed, as can be seen in Fig. 5(c), and new particles get in contact with the cooler gas entering the bed, following the bed dynamics detailed in Section 4.1. This intimate mixing and agitation result in a uniform temperature distribution throughout the bed, as can be seen after a few seconds at Fig. 5(e).

In addition to the enhanced heat and mass transfer capability of fluidized beds, the mixing is one of the main advantages of using fluidized beds in industrial processes. In case of nuclear bed reactors, this mixing acts reducing the hot-spot factor and yielding a high temperature of fluid without leading to an excessive fuel temperature. For the same reasons, there results an even, and consequently high, burnup of all the fuel, irrespective of the shape of the neutron-flux distribution.

The temperature of the particles was monitored over time and an average value for the bed temperature, T_{bed} was calculated at each time step. Figure 6 shows the evolution of the bed temperature along time. It is worth mentioning that the Young's modulus adopted to model the particles ($10^7 N/m^2$) in this work is small compared to real value for common materials (which can be easily higher than $10^9 N/m^2$). Although it is quite common to artificial softening the particles for isothermal applications, since it does not impact post and pre-collision velocities and therefore do not significantly affect the solution acuracy (of course, avoiding extreme softening in order to not affect non-real deformations), for systems in which heat transfer is solved this can introduce significant errors. With the augment of the particle stiffness, both the contact duration and particle contact area are increased, which act to increase conductive heat transfer between colliding particles.

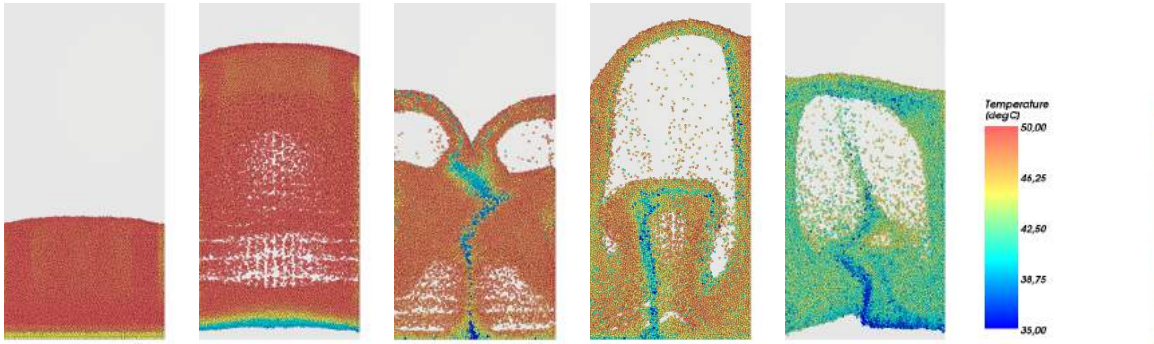

(a) 1s (b) 2 s (c) 3 s (d) 5 s (e) 10 s

Figure 5: Temperature of the particles at 1, 2, 3, 5 and 10s of simulation.

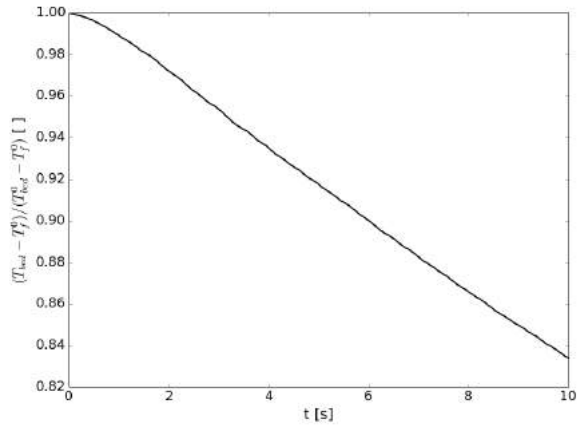

Figure 6: Evolution of average bed temperature.

However, using realistic model parameters is unfeasible for large-scale simulation due to the high computational costs (the greater the particle stiffness, the smaller the time step). As the next step, the correction terms recently proposed by Morris *et al.* (2016) to eliminate the impact that artificial softening has on the simulated heat transfer are going to be implemented, enabling the usage of collision softening to reduce computational cost without adverse effect on heat transfer for dense systems.

5. CONCLUSIONS

In this work, coupling between DEM and CFD packages Rocky® and ANSYS Fluent® was implemented and demonstrated through a numerical example. Mathematical modeling was presented, focusing on DEM, CFD and the coupling methods. The CFD-DEM coupling was applied to the simulation of a bubbling fluidized bed and the numerical results showed good agreement when compared to experimental data, confirming the proposed approach as a suitable alternative for modeling the fluid dynamics of fluidized bed nuclear reactors, providing detailed information of its behavior.

6. ACKNOWLEDGEMENTS

The authors acknowledge gratefully the financial support by CNPq and FAPERJ.

7. REFERENCES

Agung, A., 2007. *Conceptual design of a fluidized bed nuclear reactor, statics, dynamics and safety-related aspects*. Ph.D. thesis, Technische Universiteit Delft, Delft.

Bokkers, G.A., van Sint Annaland, M. and Kuipers, J.A.M., 2004. "Mixing and segregation in a bidisperse gas–solid fluidised bed: a numerical and experimental study". *Powder Technology*, Vol. 140, pp. 176–186.

Chaudhuri, B., Muzzio, F.J. and Tomassone, M.S., 2006. "Modeling of heat transfer in granular flowing rotating vessels". *Chemical Engineering Science*, Vol. 61, pp. 6348–6360.

Chiesa, M., Mathiesenb, V., Melheimc, J.A. and Halvorsend, B., 2005. "Numerical simulation of particulate flow by the eulerian–lagrangian and the eulerian–eulerian approach with application to a fluidized bed". *Computers and Chemical Engineering*, Vol. 29, pp. 291–304.

Crowe, C.T., Schwarzkopf, J.D., Sommerfeld, M. and Tsuji, Y., 2011. *Multiphase Flows with Droplets and Particles, Second Edition*. CRC Press.

Cundall, P.A. and Strack, O.D.L., 1979. "A discrete numerical model for granular assemblies". *Geotechnique*, Vol. 29, pp. 47–65.

Deen, N.G., Annaland, M.V.S., der Hoef, M.A.V. and Kuipers, J.A.M., 2007. "Review of discrete particle modeling of fluidized beds". *Chemical Engineering Science*, Vol. 62, pp. 28–44.

der Hoef, M.A.V., Ye, M., Annaland, M.V.S., Andrews, A.T., Sundaresan, S. and Kuipers, J.A.M., 2006. "Multi-scale modeling of gas fluidized beds". *Advances in Chemical Engineering*, Vol. 31, p. 65.

Drew, D., 1993. "Mathematical modeling of two-phase flow". *Annual Review of Fluid Mechanics*, Vol. 15, pp. 261–291.

Gidaspow, D., 1994. *Multiphase Flow and Fluidization*. Academic Press, San Diego.

Gidaspow, D., 2012. *Multiphase Flow and Fluidization: Continuum and Kinetic Theory Descriptions*. Elsevier Science.

Goldschmidt, M.J.V., Beetstra, R. and Kuipers, J.A.M., 2002. "Hydrodynamic modelling of dense gas-fluidised beds: comparison of the kinetic theory of granular flow with 3d hard-sphere discrete particle simulations". *Chemical Engineering Science*, Vol. 57, pp. 2059–2075.

Goldschmidt, M.J.V., Beetstra, R. and Kuipers, J.A.M., 2004. "Hydrodynamic modelling of dense gas-fluidised beds: comparison and validation of 3d discrete particle and continuum models". *Powder Technology*, Vol. 142, pp. 23–47.

Gunn, D., 1978. "Transfer of heat or mass to particles in fixed and fluidised beds". *Int. J. Heat Mass Transfer*, Vol. 21, pp. 467–476.

Hoomans, B.P.B., Kuipers, J.A.M., Briels, W.J. and Swaaij, W.P.M.V., 1996. "Discrete particle simulation of bubble and slug formation in a two-dimensional gas fluidised bed: a hard-sphere approach". *Chemical Engineering Science*, Vol. 51, pp. 99–118.

Hoomans, B.P.B., Kuipers, J.A.M., Salleh, M.A.M., Stein, M. and Seville, J.P.K., 2001. "Experimental validation of granular dynamics simulations of gas-fluidised beds with homogenous in-flow conditions using positron emission particle tracking". *Powder Technology*, Vol. 116, pp. 166–177.

Hoomans, B.P.B., Kuipers, J.A.M. and Swaaij, W.P.M.V., 2000. "Granular dynamics simulation of segregation phenomena in bubbling gas-fluidised beds". *Powder Technology*, Vol. 109, pp. 41–48.

Koch, D. and Hill, R., 2001. "Inertial effects in suspension and porous-media flows". *Annual Review of Fluid Mechanics*, Vol. 33, pp. 619–647.

Luo, K., Wu, F., Yang, S. and Fan, J., 2015. "Cfd–dem study of mixing and dispersion behaviors of solid phase in a bubbling fluidized bed". *Powder Technology*, Vol. 274, pp. 482–493.

Morris, A.B., Pannala, S., Ma, Z. and Hrenya, C.M., 2016. "Development of soft-sphere contact models for thermal heat conduction in granular flows". *AIChE Journal*, pp. n/a–n/a.

Ouyang, J. and Li, J.H., 2001. "Simulation of dynamic behavior in bubbling fluidization". *Progress in Natural Science*, Vol. 11, pp. 772–778.

Patil, A.V., Peters, E.A.J.F., Kolkman, T. and Kuipers, J.A.M., 2014. "Modeling bubble heat transfer in gas–solid fluidized beds using dem". *Chemical Engineering Science*, Vol. 105, pp. 121–131.

Pritchard, P.J., 2010. *Fox and McDonald's Introduction to Fluid Mechanics, 8th Edition*. John Wiley & Sons.

Sefidvash, F., 1980. "A nuclear reactor concept for brazil". *Rev. Bras. Tecnol.*, Vol. 11, p. 145.

Sefidvash, F., 1985. "A fluidized bed nuclear reactor concept". *Nuclear Technology*, Vol. 71, pp. 527–534.

Taghipour, F., Ellis, N. and Wong, C., 2005. "Experimental and computational study of gas–solid fluidized bed hydrodynamics". *Chemical Engineering Science*, Vol. 60, pp. 6857–6867.

Tsuji, Y., T, T.K. and Tanaka, 1993. "Discrete particle simulation of two-dimensional fluidized bed". *Powder Technology*, Vol. 77, pp. 79–87.

Walton, O., 1993. *Numerical simulation of inelastic, frictional particle-particle interactions*. Butterworth-Heinemann series in chemical engineering. Butterworth-Heinemann.

Xu, B.H. and Yu, A.B., 1997. "Numerical simulation of the gas-solid flow in a fluidized bed by combining discrete particle method with computational fluid dynamics". *Chemical Engineering Science*, Vol. 52, pp. 2785–2809.

Xu, B., Yu, A., Chew, S. and Zulli, P., 2000. "Numerical simulation of the gas-solid flow in a bed with lateral gas blasting". *Powder Technology*, Vol. 109, pp. 13–26.

Ye, M., der Hoef, M.A.V. and Kuipers, J.A.M., 2004. "A numerical study of fluidization behavior of geldart a particles using a discrete particle model". *Powder Technology*, Vol. 139, pp. 129–139.

Ye, M., der Hoef, M.A.V. and Kuipers, J.A.M., 2005a. "The effects of particle and gas properties on the fluidization of geldart a particles". *Chemical Engineering Science*, Vol. 60, pp. 4567–4580.

Ye, M., der Hoef, M.A.V. and Kuipers, J.A.M., 2005b. "From discrete particle model to a continuous model of geldart a particles". *Chemical Engineering Research and Design*, Vol. 83, pp. 833–843.

Yuu, S., Umekage, T. and Johno, Y., 2000. "Numerical simulation of air and particle motions in bubbling fluidized bed of small particles". *PowderTechnology*, Vol. 110, pp. 158–168.

Zhou, A.Y., Yu, A.B. and Zulli, P., 2006. "Particle scale study of heat transfer in gas fluidization". In *13rd International Heat Transfer Conference*. Sydney, Australia.

Zhou, A.Y., Yu, A.B. and Zulli, P., 2007. "Particle scale study of heat transfer in gas fluidization". In *Fourth International Conference of Discrete Element Method*. Brisbane, Australia.

Zhou, A.Y., Yu, A.B. and Zulli, P., 2010. "A new computational method for studying heat transfer in fluid bed reactors". *Powder Technology*, Vol. 197, pp. 102–110.

Zhu, H.P., Zhou, Z.Y., Yang, R.Y. and Yu, A.B., 2008. "Discrete particle simulation of particulate systems: A review of

major applications and findings". *Chemical Engineering Science*, Vol. 63, pp. 5728–5770.

8. RESPONSIBILITY NOTICE

The authors are the only responsible for the printed material included in this paper.